

# Magnetoplasmons of a two-dimensional electron gas with equilibrium density inhomogeneities

F. A. Reboredo and C. R. Proetto

*Centro Atómico Bariloche and Instituto Balseiro, Comisión Nacional de Energía Atómica, 8400 Bariloche, Argentina*

(Received 27 September 1996)

Interedge magnetoplasmons are a class of magnetoplasmons localized at the boundary defined by two bidimensional metallic domains with different equilibrium densities. They reduce to the usual edge magnetoplasmons when one of the equilibrium densities is exactly zero. The application of a hydrodynamical theory to a disk-shaped electron fluid with a central inhomogeneity reveals the existence of both edge and interedge magnetoplasmons in the high magnetic field regime, whose frequency decreases with magnetic field. If the equilibrium density of the central inhomogeneity is greater than the equilibrium density of the ring area that surrounds it, both magnetoplasmons have the same symmetry and anticross strongly. In the low-field regime, the interedge magnetoplasmon exhibits a cyclotron resonance like dependence on the magnetic field. The calculations are in qualitative agreement with recent experiments performed in the extremely high-field regime and suggest new experiments at lower fields and/or different systems. [S0163-1829(97)01719-0]

## I. INTRODUCTION AND HYDRODYNAMIC MODEL FOR A CONFINED ELECTRON FLUID

The lack of translational symmetry associated with the presence of boundaries or inhomogeneities in a system allows for the existence of effects which are qualitatively quite different from those of the bulk case. A striking example of this are the so-called edge magnetoplasmons (EMP's), which are collective density excitations of *confined* two-dimensional electron gases (2DEG's) subject to a perpendicular magnetic field.<sup>1</sup> The characteristic signature of these EMP's is that their frequency decreases with an increasing magnetic field. This contrasts with the usual bulk magnetoplasma (BMP) modes, whose squared frequency increases linearly with the squared cyclotron frequency. Besides, in the strong-field limit, EMP's are spatially localized close to the confining boundary.

Most of the experimental studies of EMP's, which include a variety of different geometric configurations, such as dots,<sup>2-4</sup> antidots,<sup>5,6</sup> and rings,<sup>7,8</sup> have been restricted to edge situations, where the equilibrium density of the confined 2DEG's changes from a finite value to zero. Theoretical studies also follow that tendency.<sup>9-18</sup> In a very recent experimental study,<sup>19</sup> however, magnetoplasmons localized at the boundary between two classical two-dimensional electron systems with different (but nonzero) equilibrium electron densities were observed. By analogy with a three-dimensional situation, where an interface is a generalization of a surface, they were denoted as interedge magnetoplasmons (IEMP's). Their existence was predicted by Mikhailov and Volkov,<sup>20</sup> who analyzed theoretically the problem of two half-plane contacting 2D metallic regions with different conductivities (densities).

Owing to the macroscopic dimensions of the typically studied samples (0.1–10 mm), we shall treat the 2DEG as a classical charged fluid subject to the laws of fluid mechanics. Generalizing on our previous model,<sup>18</sup> in the present work we will consider the case of an electron fluid confined in a disk of radius  $b$ ; the disk, however, has an inner region (of radius  $a$ ) with a static and uniform positive background with

charge density per unit area  $en_1$  ( $e>0$ ), while the annular region between  $a$  and  $b$  has background charge density  $en_2$ . The charge neutrality of the system is provided by a compressible electron fluid with area charge density  $-e[n_0(\rho) + n(\rho, t)]$ , where  $n_0(\rho) = n_1\theta(a - \rho) + n_2\theta(\rho - a)$  is the equilibrium density and  $n$  the collective mode self-induced density (we will assume that  $n \ll n_0$ ). The system is subject to a perpendicular magnetic field along the  $z$  direction and surrounded by dielectric material with dielectric constant  $\epsilon_1$  for  $z > 0$  and  $\epsilon_2$  for  $z < 0$ . This geometry corresponds quite closely with the experimental configuration of Ref. 19. Besides, it contains as a limit several previously considered models: for instance, a disk of radius  $b$  ( $a$ ) if  $n_1 = n_2$  ( $n_2 = 0$ ),<sup>1,9</sup> an antidot if  $n_1 = 0$ ,  $n_2 \neq 0$ ,  $b \rightarrow \infty$ ,<sup>12-14,16</sup> and a ring with inner radius  $a$  and outer radius  $b$  if  $n_1 = 0$ .<sup>11,15,17,18</sup>

The essential equations governing the dynamics of a compressible electron fluid within the hydrodynamical approach<sup>21</sup> are the continuity and Euler equations linearized in the velocity of the liquid  $\mathbf{v}$  and the deviation of the concentration  $n$  from its equilibrium value,  $n_0$ ,

$$\frac{\partial n(\rho, t)}{\partial t} + \nabla_\rho \cdot [n_0(\rho) \mathbf{v}(\rho, t)] = 0, \quad (1)$$

$$\frac{\partial \mathbf{v}(\rho, t)}{\partial t} - \frac{e}{m^*} \nabla_\rho \phi(\rho, t) - \omega_c \hat{\mathbf{z}} \times \mathbf{v}(\rho, t) = 0. \quad (2)$$

Here,  $\rho$  is a two-dimensional vector in the  $x$ - $y$  plane,  $\omega_c = eB/m^*c$  is the cyclotron frequency, and  $\phi$  the mode self-induced potential produced by the density fluctuation  $n$ ; it should be noted that  $\phi$  extends over all three-dimensional space (however, only its projection on the  $x$ - $y$  plane enters in the equations above), while the remaining physical magnitudes  $n_0$ ,  $n$ , and  $\mathbf{v}$  are restricted to the 2D sheet at  $z = 0$ .<sup>22</sup>

The azimuthal symmetry of our model allows us to assume that all the unknown quantities  $n$ ,  $\phi$ ,  $\mathbf{v}$  have an angular and time dependence of the form  $f(\rho) e^{i(\ell\theta - \omega t)}$ , where  $\ell$  is an

integer and  $\omega$  the frequency of the fluid normal modes, still to be found. The pair of bulk equations (1) and (2) should be supplemented by boundary conditions at the inner and outer edges at  $\rho=a$  and  $\rho=b$ , respectively; from physical arguments, we are led to choose that there is no accumulation of charge at the internal edge,  $n_1 v_\rho(\rho=a^-) = n_2 v_\rho(\rho=a^+)$ , and that the flux of charge across the external edge must be zero,  $n_2 v_\rho(\rho=b^-) = 0$ .

Using (2), these boundary conditions are mathematically equivalent to

$$n_1 \left( \omega \frac{\partial}{\partial \rho} + \frac{\ell \omega_c}{\rho} \right) \phi(\rho) \Big|_{\rho=a^-} = n_2 \left( \omega \frac{\partial}{\partial \rho} + \frac{\ell \omega_c}{\rho} \right) \phi(\rho) \Big|_{\rho=a^+}, \quad (3)$$

and

$$n_2 \left( \omega \frac{\partial}{\partial \rho} + \frac{\ell \omega_c}{\rho} \right) \phi(\rho) \Big|_{\rho=b^-} = 0, \quad (4)$$

respectively.

To proceed further, it is useful to combine Eqs. (1) and (2) in a single integrodifferential equation; after some algebra we obtain

$$\begin{aligned} (\omega^2 - \omega_c^2) n(\rho) + 4\pi\omega_0^2 \frac{n_0(\rho)}{n_2} \left( \frac{\partial^2}{\partial \rho^2} + \frac{1}{\rho} \frac{\partial}{\partial \rho} - \frac{\ell^2}{\rho^2} \right) \\ \times \int_0^b d\rho' \rho' K_\ell(\rho, \rho') n(\rho') = 0 \end{aligned} \quad (5)$$

for the self-induced electron density. The kernel  $K_\ell(\rho, \rho')$  in the equation above is given by

$$K_\ell(\rho, \rho') = \int_0^\infty J_\ell(k\rho) J_\ell(k\rho') d(kb), \quad (6)$$

with  $J_\ell$  being the  $\ell$ th order Bessel function of the first kind, while  $\omega_0^2 = e^2 n_2 / m^* b (\varepsilon_1 + \varepsilon_2)$  is a natural unit of frequency for our model. Two observations should be made concerning the derivation of Eq. (5)

(i) The boundary conditions (3) and (4) have been used to eliminate extra terms involving derivatives of the equilibrium electron density  $n_0(\rho)$ ; within our steplike model for the equilibrium density profile, such derivatives would give rise to  $\delta$  function types of charge accumulation at the edges at  $\rho=a$  and  $\rho=b$ . An alternative way of getting Eqs. (3) and (4) is to impose them as a way of avoiding such pathological (for a two-dimensional situation) localization of charge.<sup>1</sup>

(ii) The self-induced potential  $\phi(\rho)$  has been related to the self-induced density by using the integral version of the Poisson equation, which after integration over the  $z'$  coordinate reads

$$\phi(\rho) = - \frac{4\pi e}{(\varepsilon_1 + \varepsilon_2)} \int_0^b d\rho' \rho' K_\ell(\rho, \rho') n(\rho'). \quad (7)$$

At this stage, the problem has been reduced to finding the solutions of Eq. (5) subject to the boundary conditions (3) and (4); while there are several methods available to solve this problem, as in our previous work in rings we find it useful to compress these three equations into just one which satisfies automatically the boundary conditions.

Accordingly, we find it convenient to study the following integral equation:

$$\begin{aligned} \frac{e n_0(\rho)}{m^*} \phi(\rho) + (\omega^2 - \omega_c^2) \left[ \int_0^a d\rho' \rho' G_1(\rho, \rho') n(\rho') \right. \\ \left. + \int_a^b d\rho' \rho' G_2(\rho, \rho') n(\rho') \right] = 0, \end{aligned} \quad (8)$$

where  $G_1(\rho, \rho')$  and  $G_2(\rho, \rho')$  are Green's functions which satisfy different equations depending on the value of their arguments.

If  $0 \leq \rho' < a$ , we have

$$\left( \frac{\partial^2}{\partial \rho^2} + \frac{1}{\rho} \frac{\partial}{\partial \rho} - \frac{\ell^2}{\rho^2} \right) G_1(\rho, \rho') = - \frac{\delta(\rho - \rho')}{\rho'} \quad (0 \leq \rho < a), \quad (9a)$$

$$\left( \frac{\partial^2}{\partial \rho^2} + \frac{1}{\rho} \frac{\partial}{\partial \rho} - \frac{\ell^2}{\rho^2} \right) G_1(\rho, \rho') = 0 \quad (a < \rho < b), \quad (9b)$$

while if  $a < \rho' < b$ ,

$$\left( \frac{\partial^2}{\partial \rho^2} + \frac{1}{\rho} \frac{\partial}{\partial \rho} - \frac{\ell^2}{\rho^2} \right) G_2(\rho, \rho') = 0 \quad (0 \leq \rho < a), \quad (9c)$$

$$\left( \frac{\partial^2}{\partial \rho^2} + \frac{1}{\rho} \frac{\partial}{\partial \rho} - \frac{\ell^2}{\rho^2} \right) G_2(\rho, \rho') = - \frac{\delta(\rho - \rho')}{\rho'} \quad (a < \rho < b). \quad (9d)$$

With these definitions of  $G_1$  and  $G_2$ , it can easily be checked by the application of the operator  $\partial^2/\partial \rho^2 + \partial/\rho \partial \rho - \ell^2/\rho^2$  to Eq. (8) that our original Eq. (5) is obtained at once. The boundary conditions on the self-induced potential  $\phi(\rho)$  can be incorporated in turn as boundary conditions for the explicit calculation of the Green functions, this being the main practical advantage of the method. While the evaluation of  $G_1$  and  $G_2$  is, in principle, straightforward under the above guidelines, the resulting expressions are rather cumbersome, so we prefer to relegate their explicit evaluation to the Appendix.

Before embarking on a detailed numerical calculation, some comments on the results obtained so far are in order. First, it is interesting to note that while the bulk Eq. (5) remains invariant under the change  $\ell \rightarrow -\ell$ , the boundary related Eqs. (3) and (4) depend on the sign of  $\ell$  (for nonzero magnetic field). This means that when  $\omega_c \neq 0$ , bulk-type solutions should be nearly degenerate, while edge or interedge solutions should split with the magnetic field. No anomalous behavior of this sort can be expected for the  $\ell=0$  radial modes, as in this case neither the frequency nor the cyclotron frequency appears in the boundary conditions. Inspection of Eq. (5) reveals that they enter only in the particular combination  $\omega^2 - \omega_c^2$ , from which it follows that the squared frequency of these modes should increase quadratically with magnetic field, like bulk magnetoplasmons. The main consequence of confinement for the  $\ell=0$  magnetoplasmons is to give a finite value to the zero-field frequency. Physically, this qualitatively different behavior of the  $\ell=0$  modes arises from the fact that the Lorentz force gives some angular component to these radial modes. However, confinement effects (radial boundaries) are not felt by these angular components,

and the magnetic field effects are consequently similar to the bulk case. Second, solutions to Eq. (8) for a given value of  $\omega_c$  exist only for certain allowed frequencies, so this equation constitutes a generalized eigenvalue problem. The solutions  $\omega_{r,\ell}$  can be classified according to their angular momentum  $\ell$  and a sort of radial number  $r$ , such as  $\omega_{0,\ell} < \omega_{1,\ell} < \omega_{2,\ell} < \dots$ . In the numerical results to be presented below, only dipole allowed ( $\ell = \pm 1$ ) modes will be shown, for the smallest radial numbers. For our model with the magnetic field pointing along the positive direction of the  $z$  axis,  $\ell > 0$  density fluctuations rotate in the counter-clockwise sense, while negative values of the angular momentum correspond to magnetoplasmons rotating in the clockwise sense. For the practical solution of Eq. (8), we follow the same numerical technique used in Ref. 18, expanding  $n(\rho)$  into a finite set of linearly independent functions. In particular, we used as a basis  $M$  functions of the form

$$\rho^m e^{-\lambda\rho} \theta(a-\rho) \quad \text{if } 1 \leq m \leq M/2,$$

$$\rho^m e^{-\lambda\rho} \theta(\rho-a) \quad \text{if } M/2 \leq m \leq M,$$

with  $\lambda = b/M$ . All the calculations below correspond to  $M = 14$ .

## II. RESULTS

A convenient way of presenting our results is to use  $\omega_0$  as a unit of frequency, and  $b$  as a unit of length; proceeding in this way, the independent parameters of our model are  $n_1/n_2$ , the aspect ratio  $a/b$ , and the adimensional cyclotron frequency  $\omega_c/\omega_0$ . This scaling of the results allows a direct comparison of our calculations with experiments performed both in 2DEG's on the surface of liquid helium and at semiconductor heterojunctions, in spite of several order of magnitude differences in typical equilibrium densities and geometric dimensions.

Unless stated otherwise, all the results to be presented below correspond to the choice  $a/b = 0.5$  for the aspect ratio; besides, we allow  $n_1$  to change from  $n_1/n_2 \ll 1$  to  $n_1/n_2 \gg 1$ . This variation of the equilibrium density can be achieved by using the experimental techniques of Ref. 19.

We start by presenting in Fig. 1 the positive eigenfrequency solutions<sup>23</sup> for the case  $n_1/n_2 = 0$  (full and dashed lines), and  $n_1/n_2 = 0.02$  (open circles), for  $\ell = \pm 1$ . When  $n_1/n_2 = 0$ , the system reduces to the ring configuration studied in our previous work,<sup>18</sup> the main feature being that the spectrum can be characterized as a set of bulk high-frequency magnetoplasmons, and two low-frequency edge magnetoplasmons circulating along the inner ( $\ell = +1$ ) and outer ( $\ell = -1$ ) ring boundaries, in opposite directions. In the strong field limit  $\omega_c/\omega_0 \gg 1$ , they become increasingly localized close to their respective boundaries.

While for a situation with  $n_1/n_2 \ll 1$  one naively could expect to find a spectrum of collective excitations similar to the ring case, at first sight the results in Fig. 1 for  $n_1/n_2 = 0.02$  look rather different, with several additional bulk magnetoplasmons and an extra mode (for  $\ell = +1$ ) whose frequency decreases linearly with magnetic field at small fields. The extra bulk magnetoplasmons are easily characterized: they correspond to BMP of a disk of radius

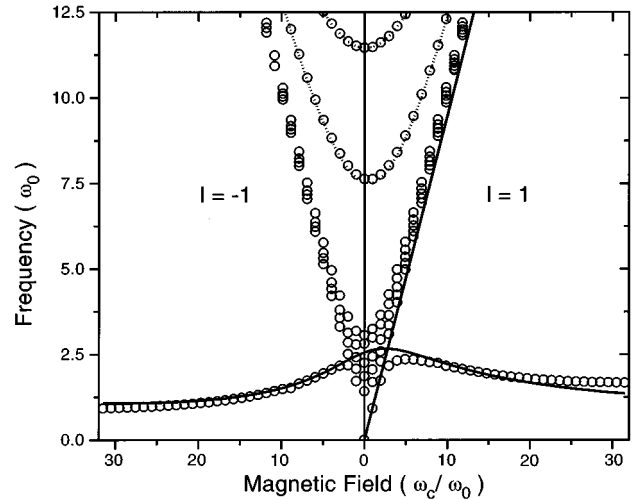


FIG. 1. Excitation spectra for a ring ( $n_1/n_2 = 0$ , full and dashed lines), and for a ringlike situation ( $n_1/n_2 = 0.02$ , open circles). The right-hand side of the figure corresponds to the  $\ell = +1$  modes, while the left-hand side is for the  $\ell = -1$  modes. The straight full line is a plot of the analytical approximation given by Eq. (10) in the text for the IEMP's in the small field regime.

$a$  and equilibrium density  $n_1$ . As  $n_1 \ll n_2$ , its zero-field frequency is much smaller than the zero-field frequency of a BMP localized in the ring region. This explains why one can excite many of these modes before exciting the first ring mode. The finite number of low-frequency BMP modes of the inner disk is just a consequence of the finite number of basis functions used in the numerical calculation. The characterization of the collective mode whose frequency goes to zero linearly with magnetic field turns out to be not so easy, at least in the zero field limit. Some help is provided by the results shown in Fig. 2, where the normalized self-induced density  $n(\rho)$  for  $n_1/n_2 = 0.02$  is shown for several magnetic fields. According to these results, this mode is localized close to the interedge (located at  $\rho/b = 0.5$ ), but while for  $\omega_c/\omega_0 \ll 1$  it is mainly localized on the inner low-density side of the interedge, when  $\omega_c/\omega_0 \gg 1$  its localization changes to the outer high-density side of the interedge. In this strong-field regime, this mode behaves essentially as the  $\ell = +1$  EMP of a ring, as can be seen clearly in Fig. 1. We still must explain the linear behavior at small magnetic fields. This behavior is related to a divergence of the Green function  $G_1(\rho, \rho')$  at a given frequency, which in turn gives rise to a divergence of the integral equation at the same frequency. A closer examination of the explicit expressions given in the Appendix reveals that  $G_1(\rho, \rho') \rightarrow \infty$  when

$$\omega = -\alpha \frac{1 - a^{2\ell}/b^{2\ell}}{1 + \alpha a^{2\ell}/b^{2\ell}} \omega_c, \quad (10)$$

with  $\alpha = (n_1 - n_2)/(n_1 + n_2)$  being an asymmetry parameter. This expression corresponds to the case  $\ell > 0$ ; for  $\ell < 0$  we should replace  $\omega_c$  by  $-\omega_c$ . If  $\ell > 0$  and  $n_1 < n_2$ , the frequency given by Eq. (10) is positive, and corresponds to the straight full line in Fig. 1. The solutions associated to the IEMP approach asymptotically this frequency (from below) as the magnetic field decreases, and this gives rise to the observed cyclotron resonance behavior of this mode at small

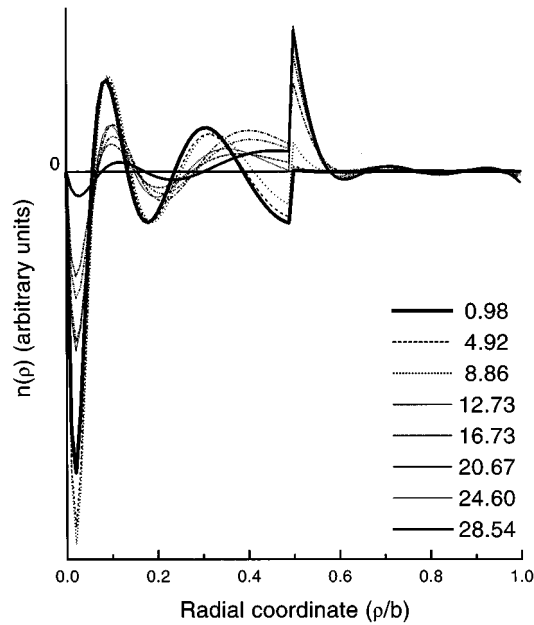


FIG. 2. Radial profile of the IEMP self-induced density for several values of the magnetic field, for a ringlike configuration  $n_1/n_2=0.02$ . The magnetic field varies from  $\omega_c/\omega_0=0.98$  to  $\omega_c/\omega_0=28.54$ , in steps of 3.96.

fields. It is clear that the Coulomb interaction is irrelevant for this mode, since the integral equation is dominated by the singularity in  $G_1$ . It is interesting to point out that in the limit  $b \rightarrow \infty$  (antidot configuration), Eq. (10) reduces to the one found by Mikhailov and Volkov<sup>20</sup> for the IEMP in a rectilinear half-plane geometry. In that case, this mode arises from the anticrossing of the cyclotron resonance mode and the IEMP oscillation.

We display in Fig. 3 the spectrum of  $\ell = \pm 1$  collective

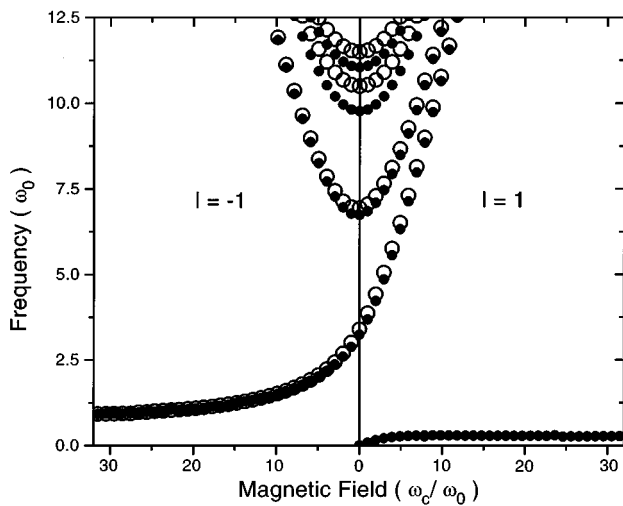


FIG. 3. Resonance frequencies for a disklike configuration with  $n_1/n_2=0.8$  (full circles). Note the softening of the IEMP as the interedge equilibrium density discontinuity is small as compared with the previous ring and ringlike case of Figs. 1 and 2. Open circles correspond to the excitation spectra for a disk with homogeneous equilibrium density  $n_1/n_2=1$ .

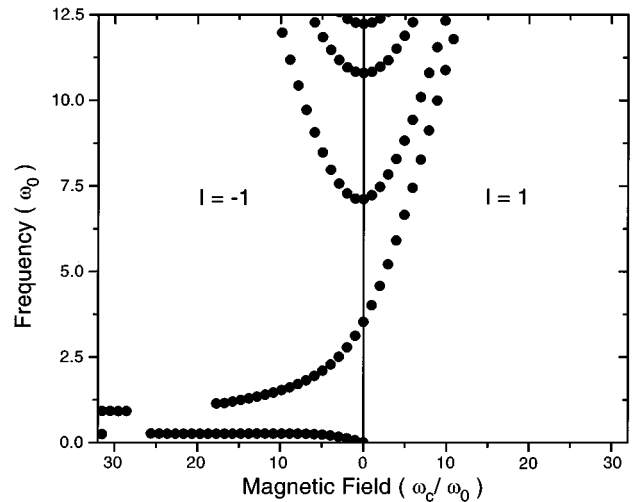


FIG. 4. Resonance frequencies for a disklike configuration  $n_1/n_2=1.2$ . Note the presence of a low-frequency IEMP on the  $\ell = -1$  side of the spectra. (Numerical error hinders the calculation of the resonances in some regions of the spectra.)

excitations for the case  $n_1/n_2=0.8$  (full circles). For this equilibrium density ratio the disk is close to becoming a homogeneous disk without an internal interedge. Comparing with the results shown in Fig. 1 we note a considerable softening of the IEMP; this is easily understood, as this mode is localized at the interedge, and the interedge is close to extinction. It is also interesting to note the absence of a set of low-frequency BMP as in Fig. 1, as in the present case the equilibrium density at the inner disk is similar to the one in the ring region, and consequently a BMP localized there has a frequency similar to a BMP localized in the ring region. For the sake of completeness, we give in Fig. 3 with open circles the results for the well-known limiting case of a homogeneous disk with  $n_1=n_2$ : the absence of the IEMP follows from the disappearance of the interedge at  $\rho=a$ , and only the  $\ell = -1$  EMP localized at the outer disk boundary survives in this limit.

The results presented so far correspond to situations where  $n_1 \leq n_2$ . What happens when  $n_1 > n_2$ ? The answer is given in Fig. 4, which corresponds to a ratio of equilibrium densities  $n_1/n_2=1.2$ : a new IEMP arises with  $\ell = -1$ , increasingly localized close to the interedge as the magnetic field increases. This IEMP has the same angular momentum as the EMP localized at the outer ring boundary; as we will see, this leads to interesting anticrossing effects between these two modes. To complete the sequence, Fig. 5 corresponds to the case  $n_1/n_2=5$ : the frequency of the IEMP rises with respect to the previous figure, and suffers an anticrossing with the EMP of the disk.

The case  $n_1/n_2 > 1$  can be alternatively thought of as a first (discrete) approximation to a smooth equilibrium density profile for a disk of radius  $b$ . Half-plane<sup>24,25</sup> and strip geometries<sup>26</sup> with model smooth equilibrium profiles have been studied previously, the main result being the appearance of additional acoustic modes (whose frequency goes to zero linearly with magnetic field), besides the usual EMP mode. Within this context, we can qualitatively identify the IEMP of Fig. 5 with the lowest acoustic mode of such theo-

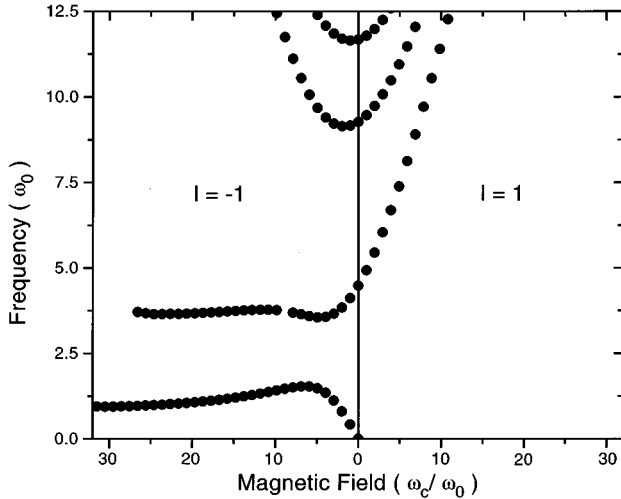


FIG. 5. Same as Fig. 4, for the case of a disk with a strong central inhomogeneity defined by  $n_1/n_2=5$ .

ries. Note, however, that in the strong magnetic field limit  $\omega_c/\omega_0 \gg 1$ , the EMP (IEMP) is mainly localized around  $b$  ( $a$ ), while for the situations considered in Refs. 24–26, all modes are localized around the same (and unique) boundary.

A complementary and quite instructive way of presenting our results is to keep the magnetic field fixed, and changing the ratio  $n_1/n_2$ ; results for the two-lowest edge and inter-edge magnetoplasmons are presented following this procedure in Fig. 6. Full and open circles correspond to a weak magnetic field regime  $\omega_c/\omega_0 \ll 1$ . The upper branch, with angular momentum  $\ell = -1$ , is associated with the collective

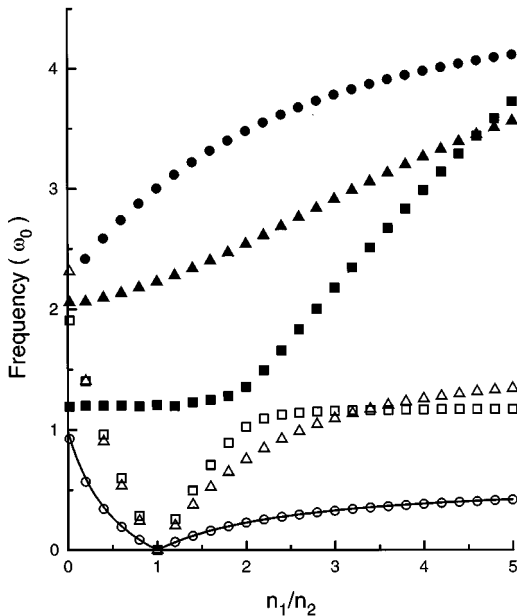


FIG. 6. Frequencies of the EMP's (full points) and the IEMP's (open points), as a function of  $n_1/n_2$ ; circles, triangles, and squares correspond to  $\omega_c/\omega_0 = 0.98, 3.92,$  and  $15.68$ , respectively. Note the strong anticrossing at  $n_1/n_2 \approx 2$ , and that this mode repulsion decreases with magnetic field. The full line on the results for the smaller field is the analytical approximation given by Eq. (10) in the text to the IEMP's.

excitation which in the strong field regime we identify as the EMP's mainly localized at the outer disk boundary. The important monotonic increase of this mode frequency with  $n_1$  confirms that this mode spreads all over the disk area in this small field regime, and consequently becomes sensitive to changes in  $n_1$ . The lower V-shaped branch corresponds to the IEMP's (at least in the strong-field regime); its angular momentum is positive (+1) if  $n_1 < n_2$ , and negative (-1) if  $n_1 > n_2$ . Besides, as discussed above, its frequency goes to zero at the homogeneous disk limit  $n_1 = n_2$ . Note that the first calculated point for this branch (in the small-density limit) is  $n_1/n_2 = 0.02$  (in agreement with the results of Fig. 1). Finally, the full line corresponds to Eq. (10), which clearly becomes an excellent analytical approximation for the frequency of the mode in this regime. Using this equation we obtain in the low-density limit  $n_1/n_2 \rightarrow 0$  the frequency  $\omega_c$ , while in the high-density  $n_1/n_2 \rightarrow \infty$  the mode frequency tends to  $\omega_c(1 - a^2/b^2)/(1 + a^2/b^2) = 0.6 \omega_c$  for our particular choice  $a/b = 0.5$ .

Finally, the remaining points in Fig. 6 are a recopilation of data for increasing magnetic field values. The most remarkable feature is the strong anticrossing between the two modes with  $\ell = -1$  on the high-density side  $n_1/n_2 > 1$ . Note that when  $n_1/n_2 < 1$ , both modes have different angular momentum and then they cross perfectly. It is also interesting to note that the strength of the anticrossing diminishes with the magnetic field. This is easily understood: when the magnetic field increases both the EMP's and the IEMP's become increasingly localized in their respective boundaries. This increasing localization is obviously detrimental to their mutual interaction, and consequently to the anticrossing effect.

### III. DISCUSSION OF THE RESULTS AND CONCLUSIONS

The results obtained in the present contribution give a rather complete picture of the collective excitations of 2DEG localized at the boundary between two regions with different equilibrium densities. This situation may be realized experimentally by the application of gates to electrons confined to the surface of liquid helium,<sup>19</sup> by etch processing of a  $\text{Al}_x\text{Ga}_{1-x}\text{As}/\text{GaAs}$  quantum well heterostructure,<sup>7</sup> or arise naturally in both kinds of systems as a result of a sample inhomogeneity.

The first point to note is that, according to the results presented in Fig. 1, the  $n_1/n_2 \rightarrow 0$  limit of our model is qualitatively different from the case  $n_1/n_2 = 0$  (the ring case). The limit  $n_1/n_2 \ll 1$  (but nonzero), allows for the presence of a set of low-frequency bulk magnetoplasmons mainly localized at the inner disk. When  $n_1/n_2 = 0$ , the remaining modes are only those localized in the high-density ring region.

One important parameter that controls the collective excitation spectra is the ratio between inner and outer equilibrium densities: if  $n_1/n_2 < 1$ , we have a ringlike situation, with two localized magnetoplasmons in the high-field regime, one at the outer boundary ( $\ell = +1$ ), and the other at the inner boundary ( $\ell = -1$ ). The frequency of the last mode goes to zero when  $n_1/n_2 \rightarrow 1$ . The case  $n_1/n_2 > 1$  is quite different: we have again two localized magnetoplasmons (in the strong-field limit), one localized at the outer boundary, the other at the inner boundary, but this time both

modes have the same symmetry (angular momentum). This gives rise to the interesting effect of the anticrossing of both modes, as can be seen clearly in Fig. 6. This anticrossing is obviously absent if  $n_1/n_2 < 1$ , and the effect diminishes by increasing magnetic field, due to the increasing localization of each mode at its respective boundary. This leads us directly to the discussion of the possible experimental detection of these features.

To the best of our knowledge, there is only one published experimental work devoted to explore the physics of IEMP's.<sup>19</sup> The 2DEG in question consists of electrons confined to a cylindrical cell and floating on the surface of liquid helium. In the high magnetic field limit the frequency of these IEMP's was found to be proportional to the difference of the electron densities on either side of the boundary and inversely proportional to the magnetic field. Also, the direction of propagation was determined by the sign of the difference  $n_1 - n_2$ . All these features are in qualitative agreement with our theoretical findings. However, it is quite important to note that the equilibrium densities and magnetic fields in the experiment are quite different from ours; a useful parameter that comprises such differences is the adimensional ratio  $\omega_c/\omega_0$ . Taking from the experiment  $n_2 \approx 6 \times 10^{17}/\text{cm}^2$ ,  $\varepsilon_1 = 1$  (vacuum),  $\varepsilon_2 \approx 1$  (liquid helium),  $b \approx 6$  mm, and assuming  $m^* = m_0$  for electrons above liquid helium ( $m_0$  being the electron bare mass), we obtain  $\omega_c/\omega_0 \approx 2000$  in the high-field limit ( $B \approx 5$  T). These experimental results are consequently far away (in the extremely high-field limit) from the calculations presented above, where  $\omega_c/\omega_0$  takes a maximum value of about 10. Not quite surprisingly, and presumably due to the strong spatial localization of the EMP's and IEMP's in this extremely high-field regime, no anticrossing of both modes was detected experimentally. It would be interesting, accordingly, to repeat the experiment under smaller magnetic fields, where  $\omega_c$  and  $\omega_0$  are about of the same order of magnitude. From  $\omega_c \approx \omega_0$ , we estimate that experiments performed to  $B \approx 0 - 100$  G will display the rich spectrum shown above.

A second possibility is to perform the experiment on a 2DEG at the interface between two semiconductors, such as GaAs and  $\text{Al}_x\text{Ga}_{1-x}\text{As}$ . Subsequent etching allows us to confine these in principle infinite two-dimensional electron gases to geometries such as disks, rings, stripes, etc. Typical parameters for these systems are much higher densities, and smaller geometric dimensions; for example, from Ref. 7, with  $n_2 = 2.3 \times 10^{11}/\text{cm}^2$ ,  $\varepsilon_1 = 1$  (vacuum),  $\varepsilon_2 = 12.6$  (GaAs),  $b = 25 \mu\text{m}$ , and  $m^* = 0.067m_0$ , we obtain  $\omega_c/\omega_0 \approx 20$ , again for  $B \approx 5$  T. We expect that the results presented here can be in consequence quantitative compared with experiments in these semiconductor heterostructures. This is supported by the results of two recent calculations for the ring case<sup>17,18</sup> that show an excellent quantitative agreement with the corresponding experiment.<sup>7</sup>

#### ACKNOWLEDGMENTS

One of the authors (F.A.R.) is indebted to CONICET of Argentina for financial support, and we thank V. Grunfeld for a careful reading of the manuscript.

#### APPENDIX A: CALCULATION OF THE GREEN'S FUNCTIONS

The calculation of the Green's functions  $G_1(\rho, \rho')$  and  $G_2(\rho, \rho')$  proceeds as follows. To begin with, they should satisfy Eqs. (9a)–(9d) given above; besides, we need a suitable set of boundary conditions for these Green functions at both interfaces. To deduce such boundary conditions, we particularize Eq. (8) for  $\rho = a^-$  and  $\rho = a^+$ ,

$$\frac{en_1}{m^*} \phi(a^-) + (\omega^2 - \omega_c^2) \left[ \int_0^a d\rho' \rho' n(\rho') G_1(a^-, \rho') + \int_a^b d\rho' \rho' n(\rho') G_2(a^-, \rho') \right] = 0, \quad (\text{A1})$$

and

$$\frac{en_2}{m^*} \phi(a^+) + (\omega^2 - \omega_c^2) \left[ \int_0^a d\rho' \rho' n(\rho') G_1(a^+, \rho') + \int_a^b d\rho' \rho' n(\rho') G_2(a^+, \rho') \right] = 0. \quad (\text{A2})$$

The application of the electrostatic requirement  $\phi(a^-) = \phi(a^+)$  to Eqs. (A1) and (A2) yields

$$\frac{1}{n_1} G_i(a^-, \rho') = \frac{1}{n_2} G_i(a^+, \rho'), \quad (\text{A3})$$

with  $i = 1, 2$ .

In a quite analogous way, the application of the boundary conditions (3) and (4) to Eq. (8) leads to the following requirements on the Green functions:

$$\left( \omega \frac{\partial}{\partial \rho} + \frac{\ell \omega_c}{\rho} \right) G_i(\rho, \rho') \Big|_{\rho=a^-} = \left( \omega \frac{\partial}{\partial \rho} + \frac{\ell \omega_c}{\rho} \right) G_i(\rho, \rho') \Big|_{\rho=a^+}, \quad (\text{A4})$$

and

$$\left( \omega \frac{\partial}{\partial \rho} + \frac{\ell \omega_c}{\rho} \right) G_i(\rho, \rho') \Big|_{\rho=b^-} = 0. \quad (\text{A5})$$

The problem is now well defined:  $G_1$  and  $G_2$  should satisfy the ‘‘bulk’’ equations (9a)–(9d), subject to the boundary conditions (A3)–(A5) at the interfaces. Generalizing previous similar derivations for different geometries,<sup>9,10,18</sup> it is not hard to obtain the following explicit expressions for the Green functions:

$$G_1(\rho, \rho') = \begin{cases} \rho' \left( \frac{A}{D} \rho'^{\ell} + \rho'^{-\ell} \right) / 2\ell, & \rho < \rho' < a \\ \rho' \left( \frac{A}{D} \rho^{\ell} + \rho^{-\ell} \right) / 2\ell, & \rho' < \rho < a \\ \rho' \left( \frac{B}{D} \rho^{\ell} + \frac{C}{D} \rho^{-\ell} \right) / 2\ell, & a < \rho < b, \end{cases}$$

where

$$A = (\omega_c - \omega) \{-a^{-2\ell} b^{\ell-1} (\omega_c + \omega) (n_1 - n_2) + b^{-(\ell+1)} \times [n_1 (\omega_c - \omega) - n_2 (\omega_c + \omega)]\},$$

$$B = -2\omega n_2 (\omega_c - \omega) b^{-(\ell+1)},$$

$$C = 2\omega n_2 (\omega_c + \omega) b^{\ell-1},$$

$$D = (\omega_c + \omega) \{b^{\ell-1} [n_1 (\omega_c + \omega) - n_2 (\omega_c - \omega)] - a^{2\ell} b^{-(\ell+1)} (\omega_c - \omega) (n_1 - n_2)\}.$$

The corresponding expressions for  $G_2(\rho, \rho')$  are

$$G_2(\rho, \rho') = \begin{cases} \frac{1}{2\ell E} \frac{2n_1\omega}{n_1(\omega_c + \omega) - n_2(\omega_c - \omega)} \rho^{\ell} \left( \rho' - \frac{\omega_c + \omega}{\omega_c - \omega} b^{2\ell} \rho'^{-\ell} \right), & \rho < a < \rho' < b \\ \frac{1}{2\ell E} \left( \rho^{\ell} - \frac{(\omega_c + \omega)(n_1 - n_2)}{n_1(\omega_c + \omega) - n_2(\omega_c - \omega)} a^{2\ell} \rho^{-\ell} \right) \left( \rho' - \frac{\omega_c + \omega}{\omega_c - \omega} b^{2\ell} \rho'^{-\ell} \right), & a < \rho < \rho' < b \\ \frac{1}{2\ell E} \left( \rho^{\ell} - \frac{\omega_c + \omega}{\omega_c - \omega} b^{2\ell} \rho^{-\ell} \right) \left( \rho' - \frac{(\omega_c + \omega)(n_1 - n_2)}{n_1(\omega_c + \omega) - n_2(\omega_c - \omega)} a^{2\ell} \rho'^{-\ell} \right), & a < \rho' < \rho < b, \end{cases}$$

with

$$E = (\omega_c + \omega) \left[ \frac{a^{2\ell} (n_1 - n_2)}{n_1(\omega_c + \omega) - n_2(\omega_c - \omega)} - \frac{b^{2\ell}}{\omega_c - \omega} \right].$$

These general expressions reduce to that obtained in previous works when the corresponding limits are taken. For ex-

ample, it can easily be checked that if  $n_1 = n_2$  we obtain a set of equations which describes a disk of radius  $b$  with a homogeneous equilibrium density.<sup>9</sup> Also, by taking  $n_1 = 0$ , the system of equations reduces to that corresponding to a ring with inner (outer) radius  $a$  ( $b$ ) and equilibrium density  $n_2$ .<sup>18</sup>

- <sup>1</sup>V. A. Volkov and S. A. Mikhailov, Zh. Éksp. Teor. Fiz. **94**, 217 (1988) [Sov. Phys. JETP **67**, 1639 (1988)].
- <sup>2</sup>S. J. Allen, H. L. Stormer, and J. C. M. Hwang, Phys. Rev. B **28**, 4875 (1983).
- <sup>3</sup>D. B. Mast, A. J. Dahm, and A. L. Fetter, Phys. Rev. Lett. **54**, 1706 (1985).
- <sup>4</sup>D. C. Glatli, E. Y. Andrei, G. Deville, J. Poitrenaud, and F. I. B. Williams, Phys. Rev. Lett. **54**, 1710 (1985).
- <sup>5</sup>K. Kern, D. Heitmann, P. Grambow, Y. H. Zhang, and K. Ploog, Phys. Rev. Lett. **66**, 1618 (1991).
- <sup>6</sup>Y. Zhao, D. C. Tsui, M. Santos, M. Shayegan, R. A. Ghanbari, D. A. Antoniadis, and H. I. Smith, Appl. Phys. Lett. **60**, 1510 (1992).
- <sup>7</sup>C. Dahl, J. P. Kotthaus, H. Nickel, and W. Schlapp, Phys. Rev. B **48**, 15 480 (1993).
- <sup>8</sup>P. J. M. Peters, P. K. H. Sommerfeld, S. van den Berg, P. P. Steijaert, R. W. van der Heijden, and A. T. A. M. de Waele, Physica B **204**, 105 (1995).
- <sup>9</sup>A. L. Fetter, Phys. Rev. B **32**, 7676 (1985); **33**, 3717 (1986); **33**, 5221 (1986).
- <sup>10</sup>V. Cataudella and G. Iadonisi, Phys. Rev. B **35**, 7443 (1987).
- <sup>11</sup>C. R. Proetto, Phys. Rev. B **46**, 16 174 (1992).
- <sup>12</sup>V. Fessatidis, H. L. Cui, and O. Kühn, Phys. Rev. B **47**, 6598 (1993).
- <sup>13</sup>K. Tevosyan and V. Shikin, Zh. Éksp. Teor. Fiz. **104**, 4121 (1993) [Sov. Phys. JETP **77**, 993 (1993)].

- <sup>14</sup>G. Y. Wu and Y. Zhao, Phys. Rev. Lett. **71**, 2114 (1993).
- <sup>15</sup>H. L. Cui, V. Fessatidis, and O. Kühn, Superlatt. Microstruct. **17**, 173 (1995).
- <sup>16</sup>S. A. Mikhailov and V. A. Volkov, Phys. Rev. B **52**, 17 260 (1995).
- <sup>17</sup>E. Zaremba, Phys. Rev. B **53**, R10 512 (1996).
- <sup>18</sup>F. A. Reboredo and C. R. Proetto, Phys. Rev. B **53**, 12 617 (1996).
- <sup>19</sup>P. K. H. Sommerfeld, P. P. Steijaert, P. J. M. Peters, and R. W. van der Heijden, Phys. Rev. Lett. **74**, 2559 (1995).
- <sup>20</sup>S. A. Mikhailov and V. A. Volkov, J. Phys. Condens. Matter **4**, 6523 (1992).
- <sup>21</sup>S. Lundqvist, in *Theory of the Inhomogeneous Electron Gas*, edited by S. Lundqvist and N. H. March (Plenum, New York, 1983).
- <sup>22</sup>A. L. Fetter, Ann. Phys. (N.Y.) **81**, 367 (1973); **88**, 1 (1974).
- <sup>23</sup>Inspection of Eqs. (3), (4), and (5) reveals the if  $\omega \geq 0$  is a solution for a given  $\omega_c$ ,  $-\omega$  is solution for  $-\omega_c$ . As both positive and negative frequencies correspond physically to the same fluctuation density, we concentrate only on the positive solutions.
- <sup>24</sup>S. S. Nazin and V. B. Shikin, Zh. Éksp. Teor. Fiz. **94**, 133 (1988) [Sov. Phys. JETP **67**, 288 (1988)].
- <sup>25</sup>I. L. Aleiner and L. I. Glazman, Phys. Rev. Lett. **72**, 2935 (1994).
- <sup>26</sup>I. L. Aleiner, Dongxiao Yue, and L. I. Glazman, Phys. Rev. B **51**, 13 467 (1995).